A polarizability driven *ab initio* molecular dynamics approach to stimulating Raman activity: Application to C_{20}

Dominick Pierre-Jacques[1], Ciara Tyler[1], Jason Dyke[1], Alexey L. Kaledin[2] and Martina Kaledin[1,*]
[1] *Department of Chemistry & Biochemistry, Kennesaw State University, 370 Paulding Ave NW, Box # 1203, Kennesaw, GA 30144*
[2] *Cherry L. Emerson Center for Scientific Computation, Emory University, 1515 Dickey Drive, Atlanta, Georgia, 30322*

Abstract: We describe a novel variant of the driven molecular dynamics (DMD) method derived for probing Raman active vibrations. The method is an extension of the conventional μ-DMD formulation for simulating IR activity by means of coupling an oscillating electric field to the molecule's dipole moment, μ, and inducing absorption of energy via tuning the field to a resonant frequency. In the present work, we modify the above prescription to invoke Raman activity by coupling two electric fields, i.e., a "Pump" photon of frequency ω_P and a Stokes photon of frequency ω_S to the molecule's polarizability tensor, $\boldsymbol{\alpha}$, with the difference in the frequencies of the two photons $\omega = \omega_P - \omega_S$ corresponding to the Stokes Raman shift. If a particular ω is close to a Raman active vibrational frequency, energy absorption by the molecule ensues. Varying ω over the desired frequency range allows identifying and assigning all Raman active vibrational modes, including anharmonic corrections, in the range by means of trajectory analysis. We show that only one element of the full polarizability tensor, and its nuclear derivative, is needed for an α-DMD trajectory, making this method well suited for *ab initio* dynamics implementation. Numerical results using first-principles calculations are presented and discussed for the vibrational fundamentals, combination bands, overtones of H_2O, CH_4, and the C_{20} fullerene.

TOC graphics

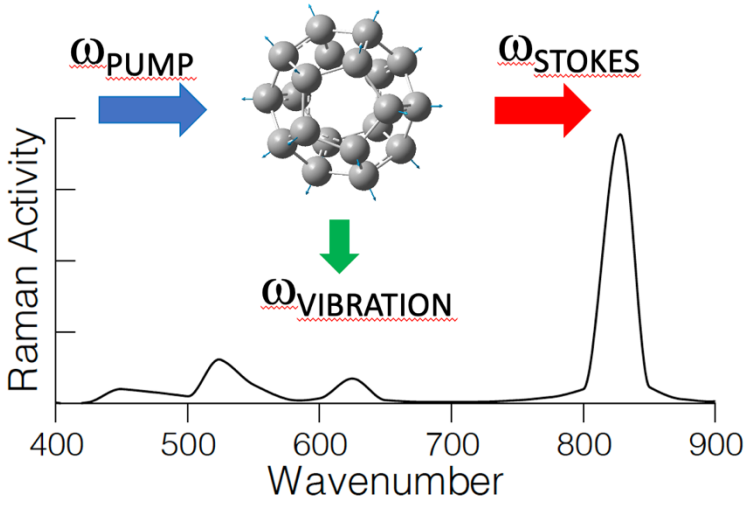

KEYWORDS: Driven molecular dynamics; polarizability tensor surface; stimulated Raman excitation; molecular vibrations; electronic structure theory

1. Introduction

Driven molecular dynamics (DMD) has recently become a powerful tool for calculating and assigning infrared (IR) spectra. Its robustness is a direct consequence of DMD's formulation, where an external time-dependent driving potential $\vec{\mu} \cdot \vec{\varepsilon}(t)$ is added to the Hamiltonian ($\vec{\mu}$ is the dipole and $\vec{\varepsilon}(t)$ is the electric field), and resonant energy absorption is duly invoked by choosing the field's frequency close to a system's vibrational frequency. This was first aptly demonstrated in single and double-laser IR multiphoton absorption (MPA) simulations of diatomics. [1-5] More recently, it has been demonstrated on polyatomic molecules, as well as peptides and small proteins, that DMD can routinely identify fundamentals, combination bands, overtones, and their anharmonic shifts by the effort of propagating classical trajectories. [6-14] Particularly attractive features of the dipole-driven MD, or μ-DMD, include the capability for assignment of vibrational spectra [15] and a straightforward way to design pump-probe 'virtual' 2D experiments. [9] Additionally, Fermi-like resonances have been observed, [10,14] and IR peaks arising due to strong non-linearity of the dipole moment in shared-proton systems have been described. [12] Furthermore, the ability of DMD to sample the low frequency parts of vibrational spectra, i.e. in the far IR and terahertz regimes, can be especially useful in studies of biological macromolecules and liquid phase simulations, as was demonstrated by bond-driving a water solvated dialanine. [16] Yet despite these attractive characteristics of DMD, so far only dipole active vibrational spectra, i.e. linear and 2D-IR, have been studied rigorously. In the present paper, we extend the formalism of DMD to electric field-polarizability interaction, calling it α-DMD, and demonstrate its applicability to calculating vibrational Raman activities on real systems.

Recent work on N_2H^+…OC shows that it is possible to carry out μ-DMD simulations directly using *ab initio* potential energy and dipole moment surfaces, PES and DMS respectively,

and their derivatives, without making approximations beyond the level of electronic structure theory for these quantities. [14] This may potentially be particularly important for α-DMD simulations, since accurate *ab initio* level analytical representation of a polarizability tensor surface for a generic polyatomic molecule or cluster is expected to be more challenging than, for instance, that of potential energy or dipole moment surfaces, as is done using the invariant polynomial approach. [17] In fact, in the literature, the presently used analytical treatment of molecular polarizability is based mainly on empirical models. [18-21] Substantially more advanced and practically successful treatments of the polarizability tensor at a high *ab initio* level, using truncated many-body expansions of monomer interactions, have been employed in the special case of liquid water. [22,23] Plane wave DFT direct molecular dynamics simulations have been carried out for calculating polarizability-polarizability correlation functions and Raman spectra in liquid and solid phases using analytical methods for the polarizability tensor, [24-27] however, a post SCF/non-DFT calculation of the full polarizability tensor at a molecular configuration along the trajectory requires at least six additional dipole calculations, for example by electric field finite-differences method. For some non-variational electronic structure methods, e.g., MP2, CCSD, etc., a dipole calculation also requires evaluation of the energy gradient, making direct *ab initio* trajectory calculations using these highly accurate methods computationally quite inefficient. However, as we will show below, to propagate an α-DMD trajectory "on the fly" using a generic electronic structure method, only two additional energy gradient calculations per time step are required, allowing this method to scale identically to μ-DMD.

As is the case with μ-DMD, all Raman active transitions beyond the usual fundamentals can be detected with α-DMD by scanning or gauging, over the driving frequency. Namely, combination bands and overtones can be captured within the usual classical limit, while purely

quantum effects, such as tunneling, energy and angular momentum quantization obviously cannot. Additionally, diagonal anharmonicities and anharmonicities resulting from mode interactions can be readily described. We note, however, that unlike the conventional MD approaches to calculating spontaneous Raman scattering spectra using polarizability-polarizability correlation functions, [28] α-DMD uses both the incident (Pump) and scattered (Stokes) lights as input to induce absorption of energy by driving the molecule at the difference frequency. Thus, in the present calculations, we do not measure 'exact' depolarization ratios as is done in MD simulations or a normal mode analysis. [29] However, we do examine the molecule's dynamical response to the driving fields in the two polarization regimes: parallel and perpendicular. A driven trajectory yields characteristic atomic displacements at resonant frequencies, similar to normal modes, [7,9,15] which contain full information about the vibrational motion. In short, in α-DMD, one not only generates a spectrum as one does from the correlation function methods, [24-27] but also assigns it using simple trajectory analysis.

The rest of the paper presents a detailed theoretical derivation of the method followed by several numerical examples to demonstrate the "proof of principle" of α-DMD. We continue the presentation by demonstrating DMD-induced Raman activity on a small, quasi-spherical fullerene, C_{20}. Perspective facility of α-DMD in designing mixed pump-probe virtual experiments, including Raman-Raman, Raman-IR and IR-Raman types, is briefly explored in the Conclusions. Additional theoretical support of the underlying theory and methodology is provided in the Supplementary Information (SI).

2. Theory

In molecular dynamics driven by an electric field, the system Hamiltonian H_0, which represents the 'internal' system energy, is appended with a time-dependent 'external' energy term,

$$H(\mathbf{p},\mathbf{q},t) = H_0(\mathbf{p},\mathbf{q}) + W(\mathbf{q},t) \quad (1)$$

where **p** and **q** are the conjugate momenta and coordinates, i.e., 3*N* Cartesians for *N* atoms. In a weak electric field regime, [30] the external energy may be written out in the order of electric field $\vec{\varepsilon}$ powers

$$W(\mathbf{q},t) = W_1(\mathbf{q},t) + W_2(\mathbf{q},t) + \cdots \quad (2)$$

where the first-order contribution is the dipole-field energy,

$$W_1(\mathbf{q},t) = \vec{\mu}(\mathbf{q}) \cdot \vec{\varepsilon}(t) \quad (3)$$

the second-order contribution is the induced dipole-field energy, i.e., the polarizability,

$$W_2(\mathbf{q},t) = \frac{1}{2}\vec{\varepsilon}(t) \cdot \boldsymbol{\alpha}(\mathbf{q}) \cdot \vec{\varepsilon}(t) \quad (4)$$

etc. [31]

It has been shown extensively in several recent publications that driving the molecule with the dipole term (W_1) produces energy absorption at resonant frequencies and allows one to construct a complete IR spectrum of the molecule. [10-14] Moreover, the recorded vibrational motions at the resonant driving frequencies provide characteristic signatures that can be used to make unambiguous assignments. Namely, taking the electric field as a sinusoidal wave and substituting it into Eq. 3 yields the well-known expression for the dipole-field driven energy term,

$$W_1(\mathbf{q},t) = |\vec{\varepsilon}|\mu_\varepsilon(\mathbf{q})\cos(\omega t + \phi) \quad (5)$$

where the scalar μ_ε is the full dipole's projection on the electric field unit vector. (Note that the choice of phase is arbitrary and is usually taken as $\phi = 0$ or $\pm\pi/2$.) [2-5,13,14] Below, we consider a similar approach to driving a molecule while using the induced dipole term (W_2) and with two

independent field vectors, as input, oscillating at different frequencies. One field acts as a pump photon, and the other acts as a probe photon, in a manner formally similar to a stimulated Raman scattering process. Such an approach based on a pump-probe light driven harmonic oscillator has been discussed previously in time-resolved studies of molecular vibrations and in studies of vibrational dynamics of liquids and solids. [32,33]

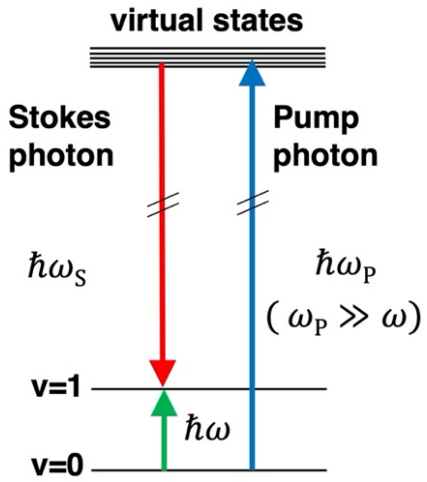

Scheme 1. A DMD interpretation of a stimulated (Pump-Stokes) Raman scattering experiment for a fictitious 2-level molecule, in the initial vibrational state v=0 and with ω_P the Pump light frequency and ω_S the Stokes light frequency (blue and read arrows). When the difference in Pump-Stokes frequencies ω_P - ω_S corresponds to the fundamental vibrational transition frequency (green arrow), v=0 → v=1, stimulated Raman excitation occurs by the process of resonantly driving the molecule at ω.

In a two-field stimulated Raman scattering experiment, in a classical setting, we assume the initial state of the molecule is the equilibrium geometry with zero initial velocities, which corresponds to the quantum ground vibrational state v=0. Therefore, we consider a Stokes shift scenario, depicted in Scheme 1, with a Pump field of frequency ω_P and a Stokes field of frequency ω_S. Treating the Pump and Stokes photons as plane polarized light, i.e., using plane waves, the total electric field interacting with the system is given by [33,34]

$$\vec{\varepsilon}(t) = \frac{1}{2}\left\{\vec{\varepsilon}_{\mathrm{P}} e^{-i(\omega_{\mathrm{P}} t + \phi_{\mathrm{P}})} + \vec{\varepsilon}_{\mathrm{S}} e^{-i(\omega_{\mathrm{S}} t + \phi_{\mathrm{S}})}\right\} + \text{c. c.} \qquad (6)$$

where $\vec{\varepsilon}_{\mathrm{P}} = \varepsilon_{\mathrm{P}}\hat{\varepsilon}_{\mathrm{P}}$ and $\vec{\varepsilon}_{\mathrm{S}} = \varepsilon_{\mathrm{S}}\hat{\varepsilon}_{\mathrm{S}}$ are the field polarization vectors. Substituting Eq. 6 into Eq. 4, the induced dipole-field energy becomes,

$$W_2(\mathbf{q}, t) = \frac{\varepsilon_{\mathrm{P}}\varepsilon_{\mathrm{S}}}{2}\alpha_{\mathrm{PS}}(\mathbf{q})\cos(\omega t + \Delta\phi) + O(2\omega_{\mathrm{P}}, 2\omega_{\mathrm{S}}, \omega_{\mathrm{P}} + \omega_{\mathrm{S}}) + const. \qquad (7)$$

where $\omega = \omega_{\mathrm{P}} - \omega_{\mathrm{S}}$ is the Stokes shift frequency, and $\Delta\phi = \phi_{\mathrm{P}} - \phi_{\mathrm{S}}$ is the phase shift between the Pump and Stokes fields. The leading term in Eq. 7 oscillates at a vibrational frequency of the molecule, by definition, is the Stokes shift. The second term is a combination of three waves, each oscillating at a vibrationally non-contributing sum-frequency. They may be omitted since by design: $2\omega_{\mathrm{P}} \approx 2\omega_{\mathrm{S}} \approx \omega_{\mathrm{P}} + \omega_{\mathrm{S}} \gg \omega$. The third term is the time-independent field-molecule interaction energy related to Rayleigh scattering activity. In the perpendicular field alignment regime, the constant term is expected to play a role in causing rotational excitation, but is presently not retained in the simulations and is subject of further investigation (see SI for more details).

For convenience, the Pump-Stokes phase shift is set to zero to make the two fields in-phase, and further, without loss of generality we require $\varepsilon_{\mathrm{P}} = \varepsilon_{\mathrm{S}} = \varepsilon_0$, leading to a computationally facilitated expression for the stimulated Raman excitation energy,

$$W_2(\mathbf{q}, t) \approx \frac{\varepsilon_0^2}{2}\alpha_{\mathrm{PS}}(\mathbf{q})\cos(\omega t) \qquad (8)$$

In Eqs. 7 and 8, $\alpha_{\mathrm{PS}}(\mathbf{q})$ is an element of the full polarizability tensor $\boldsymbol{\alpha}(\mathbf{q})$, introduced in Eq. 4, coupling the Pump and Stokes polarizations, which may be set either parallel or perpendicular to each other. It is obvious from the above that for two given polarization vectors, the Pump $\hat{\varepsilon}_{\mathrm{P}}$ and the Stokes $\hat{\varepsilon}_{\mathrm{S}}$, the scalar quantity $\alpha_{\mathrm{PS}}(\mathbf{q})$ completely determines the molecule's interaction with the field. In other words, the full polarizability tensor is not needed for the direct dynamics. Thus, for α-DMD simulations, we find it useful to denote the scalar quantity $\alpha_{\mathrm{PS}}(\mathbf{q})$ as the Polarizability

Tensor Surface (PTS), a 3*N*-6 dimensional function, in the same manner as potential energy surface (PES) and dipole moment surface (DMS) are used in the conventional MD.

We proceed with writing out Hamilton's equations of motion for the propagation of trajectories. Of interest is the differential equation for the momentum,

$$\dot{\mathbf{p}} = -\frac{\partial H}{\partial \mathbf{q}} = -\nabla V(\mathbf{q}) - \frac{\varepsilon_0^2}{2}\nabla\alpha_{\mathrm{PS}}(\mathbf{q})\cos(\omega t) \qquad (9)$$

where $V(\mathbf{q})$ is the internal potential energy, i.e., the PES. The derivative of the PTS, which we refer to as the driving force (DF), is responsible for vibrational Raman activity in the molecule. [29] As was pointed out for the case of μ-DMD above, exemplified by Eq. 5, the DF excites both vibrational and rotational motions due to the space fixed orientation of the electric field. [14] Thus, in addition to the total energy, α-DMD also leads to non-conservation of the total angular momentum during a trajectory, normally a constant of motion, which requires a careful choice of time integration step. It is important to emphasize that the form of Eq. 9 has been used for elucidating the nature of coherent optical phonons in time-resolved experiments, identifying the polarizability gradient term as cause for "stimulated Raman excitation". [35] While others, for instance, have used a differential equation identical to Eq. 9, but with a damping term, for deriving the time evolution of an ensemble vibrational coordinate in a stimulated Raman scattering setting. [32]

The DF is evaluated in the same manner as the derivative of the dipole moment, discussed previously, [14] namely, by direct numerical differentiation of the electronic energy gradient. For parallel/antiparallel Pump-Stokes polarization, with $\hat{\varepsilon}_{\mathrm{P}} \cdot \hat{\varepsilon}_{\mathrm{S}} = \pm 1$,

$$\nabla\alpha_{\mathrm{PP}} = \pm\frac{\partial^2 g}{\partial\hat{\varepsilon}_{\mathrm{P}}\partial\hat{\varepsilon}_{\mathrm{P}}} \approx \pm\frac{g(\lambda\hat{\varepsilon}_{\mathrm{P}}) + g(-\lambda\hat{\varepsilon}_{\mathrm{P}}) - 2g(0)}{\lambda^2} \qquad (10a)$$

and for perpendicular polarization, with $\hat{\varepsilon}\cdot\hat{\varepsilon}' = 0$,

$$\nabla\alpha_{\mathrm{PS}} = \frac{\partial^2 g}{\partial\hat{\varepsilon}_{\mathrm{P}}\partial\hat{\varepsilon}_{\mathrm{S}}} \approx \frac{g(\lambda\hat{\varepsilon}_{\mathrm{P}},\lambda\hat{\varepsilon}_{\mathrm{S}}) + g(-\lambda\hat{\varepsilon}_{\mathrm{P}},-\lambda\hat{\varepsilon}_{\mathrm{S}}) - g(-\lambda\hat{\varepsilon}_{\mathrm{P}},\lambda\hat{\varepsilon}_{\mathrm{S}}) - g(\lambda\hat{\varepsilon}_{\mathrm{P}},-\lambda\hat{\varepsilon}_{\mathrm{S}})}{4\lambda^2} \qquad (10b)$$

where $g(\lambda\hat{\varepsilon},\lambda\hat{\varepsilon}') \equiv \nabla V(\lambda\hat{\varepsilon},\lambda\hat{\varepsilon}')$ is the electronic energy gradient with one or two applied electric fields, and λ is an electric field differential (in practice ~30 mV/bohr). In the (anti)parallel and perpendicularly polarized α-DMD, two and four additional energy gradient calculations are required, respectively, to propagate Eq. 9 by one time step.

A typical *ab initio* calculation thus requires (*i*) a molecular structure at equilibrium and (*ii*) a choice of a single field unit vector $\hat{\varepsilon}_{\mathrm{P}}$ (parallel/antiparallel polarization) or two orthogonal unit vectors $\hat{\varepsilon}_{\mathrm{P}}$ and $\hat{\varepsilon}_{\mathrm{S}}$ in the laboratory frame. We note that it is often reasonable to evaluate the DF-PTS at a lower level of theory than the PES and its gradient to avoid computational bottlenecks, as is commonly done in similar applications. [14,36]

Given the formal similarity of the energy terms in Eqs. 5 and 8, we interpret Raman activity as molecule's absorption of the two-field energy, just as we interpret IR activity as energy absorption in a single field μ-DMD simulation. That is, resonant frequencies ω are identified by measuring the internal energy as a function of time, [7]

$$I_{\mathrm{Raman}}(\omega) = \frac{1}{\tau}\int_0^{\tau} \mathrm{d}t\, H_0(\mathbf{p}(t;\omega),\mathbf{q}(t;\omega)) \qquad (11)$$

which is expected to increase sharply on resonance and oscillate off resonance (see SI). In other words, in the α-DMD simulations, spectra are recovered by measuring energy absorption at the frequencies corresponding to the Stokes shifts. A plot of I_{Raman} vs. ω is a representation of the spectrum, with each of the resonances (peaks) described by its corresponding trajectory values $\mathbf{q}(t;\omega)$.

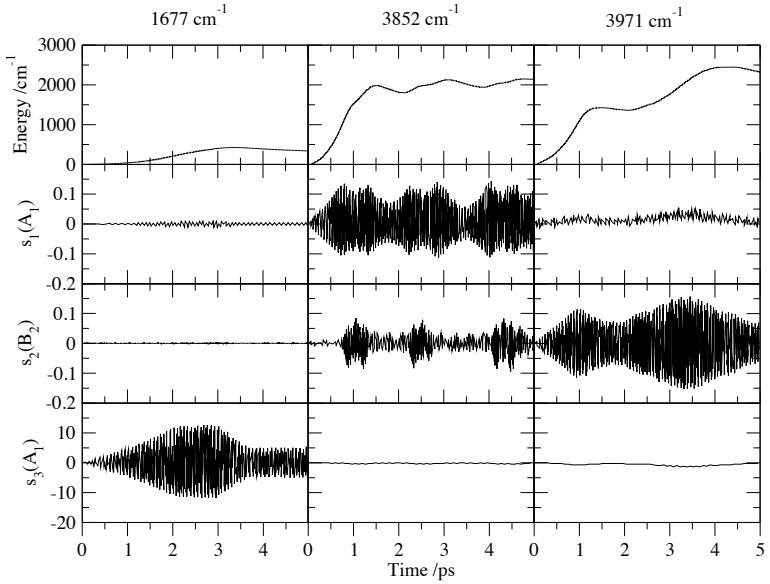

Figure 1. Direct α-DMD trajectory analysis for the Raman active H_2O fundamental frequencies $\nu_1(A_1)$=1677cm^{-1}, $\nu_2(A_1)$=3852 cm^{-1}, and $\nu_3(B_2)$=3971 cm^{-1}. Average absorbed energies are in cm^{-1}, symmetry-adapted coordinates s_1 and s_2 in Å, and s_3 in degrees. The intensity of the electric field is 500 mV/bohr. The level of theory is MP2/cc-PVDZ.

3. Computational details

The simulations presented for H_2O and CH_4 were carried out at the MP2/cc-pVDZ level of theory, sufficient for demonstration purposes and for emphasizing general applicability of the *ab initio* DMD. The simulations of C_{20} are, however, much more time consuming, and thus a less computationally demanding level of theory was chosen, namely B3LYP/6-31G(d). All geometry optimization, normal mode analysis, and IR intensities reported in this work were completed using the MOLPRO-2019.2 program [37-39], while Raman intensities were determined using the Gaussian 16 program [40]. All DMD trajectory calculations were performed using an external velocity-Verlet time integrator coupled to MOLPRO-2019.2 as the "on the fly" generator of the energy, gradient, and polarizability derivatives. We used the integration time step of 0.5 fs which in the past gave very reliable results [13,14]. To ensure accurate evaluation of Eq. 10, we use a small field differential (0.001 a.u.), which also requires that tight convergence on the electronic

wavefunction, i.e., Kohn-Sham SCF orbitals, is imposed. It was found that whereas a 10^{-8} Hartree threshold on the SCF energy is sufficient for obtaining fully converged dipole derivatives ($\nabla\mu_\varepsilon$) and PTS elements ($\alpha_{\varepsilon\varepsilon'}$) for all the systems considered presently, a 10^{-12} Hartree threshold was necessary to produce converged polarizability derivatives ($\nabla\alpha_{\varepsilon\varepsilon'}$) for C_{20}.

Presently, we run simulations in the parallel Pump-Stokes polarization regime. We analyze and plot the coordinates, driving forces, absorbed energy, etc. for the various X,Y,Z orientations of the electric field. To facilitate the assignment of spectral features, we use symmetry-adapted coordinates for H_2O and CH_4 (Eq. S4-1, S4-2 in SI), and defined the average distance of the C atoms to the center of mass $\langle R(t)\rangle$ and its fluctuation $\Delta R(t) = \sqrt{\langle R^2(t)\rangle - \langle R(t)\rangle^2}$ for C_{20}. A partial Raman spectrum of C_{20} was scanned, and the absorbed internal energy plotted as a function of frequency (Eq. 11) to identify resonant frequencies.

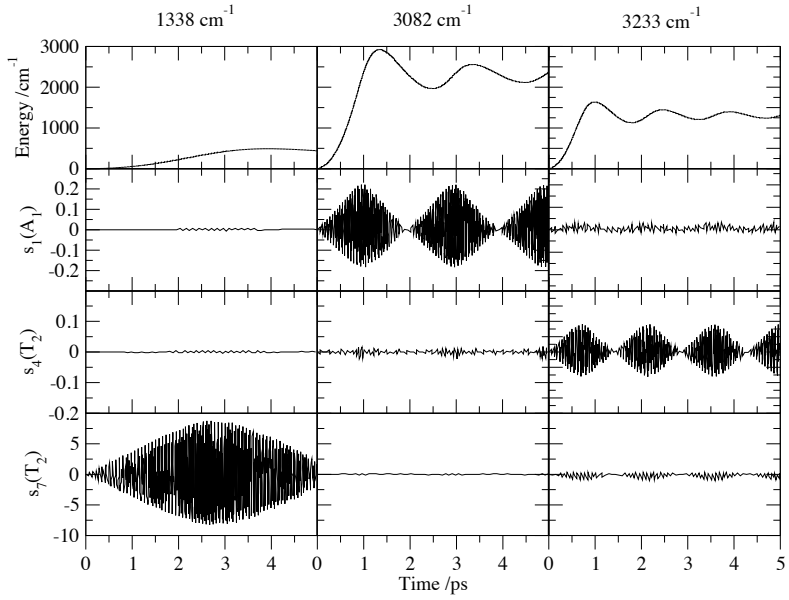

Figure 2. Direct α-DMD trajectory analysis of three of the Raman active CH_4 fundamental frequencies $\nu_1(T_2)$=1338 cm^{-1}, $\nu_3(A_1)$=3082 cm^{-1}, and $\nu_4(T_2)$=3233 cm^{-1}. The absorption energies are in cm^{-1}, symmetry-adapted coordinates, s_1 and s_4 in Å, and s_7 in degrees. The intensity of the electric field is 500 mV/bohr. The level of theory is MP2/cc-PVDZ.

4. Results and Discussion

Tables S1-S3 summarize the harmonic vibrational frequencies, IR and Raman activities, and additional data can also be found in the SI. Direct DMD simulations for H_2O and CH_4 were carried out for the fundamental frequencies, an overtone, and a combination band to demonstrate the mode assignment procedure. Since the dipole driving force is linear (Eq. 3) while the polarizability driving force is quadratic in field (Eq. 4), the field magnitude in α-DMD simulation should be stronger compared to μ-DMD to achieve comparable absorption of energy at the same resonant frequency (see also S.2 of the SI). After some exploration, the field strengths were set to 500 and 100 mV/bohr for α-DMD and μ-DMD, respectively. For an illustration, one may refer to Figure S2 which compares energy absorption regimes of Raman (α-DMD) versus IR (μ-DMD) for H_2O.

For water, all three fundamentals are IR and Raman active, which provides a good test for relative comparison of the two driving regimes. In α-DMD the two O-H stretching modes (ν_2=3852 cm^{-1} and ν_3=3971 cm^{-1}) absorb significant amounts of energy, compared to a much weaker absorption in the bending mode (ν_1=1677 cm^{-1}), as seen in Figure 1. For comparison, in μ-DMD, the asymmetric stretch and the bending mode both absorb, while the symmetric stretch is barely active (Figure S2). This is fully consistent with the quantum mechanical double harmonic approximation result. Details of the time evolution of the symmetry-adapted coordinates (s_1 symmetric stretch, s_2 asymmetric stretch, and s_3 bending) can be seen in Figure S3 of the SI.

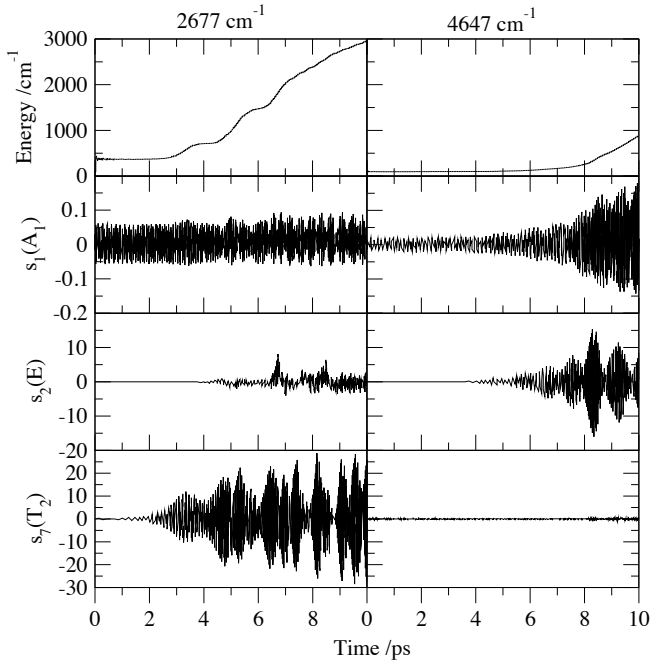

Figure 3. Direct Raman α-DMD trajectory analysis of the CH_4 overtone frequency $2\nu_1$=2677 cm^{-1} and combination band $\nu_2+\nu_3$=4647 cm^{-1}. The absorption energies are in cm^{-1}, symmetry-adapted coordinates, s_1 in Å, s_2 and s_7 in degrees. The intensities of the electric field are 1.5 V/bohr and 2.0 V/bohr, respectively. The level of theory is MP2/cc-PVDZ.

Similar coordinate analysis was carried out for some of the CH_4 fundamental modes; their resonant energy absorption is recorded in Figure 2. One can see evident excitation of the symmetry coordinate corresponding to its normal mode. We also examined two non-fundamental frequencies, one corresponding to the umbrella bending overtone $2\nu_1$=2677 cm^{-1} and the other to a combination band consisting of bending and symmetric stretch modes, $\nu_2 + \nu_3$ =4647 cm^{-1} (Figure 3). While these transitions are forbidden in the double harmonic limit, to excite them in α-DMD we used a Pump field of stronger intensity so as to induce appreciable non-linear, i.e., non-harmonic effects in both the potential and the polarizability functions. The energy profiles for these highly non-harmonic bands display certain time delays for energy absorption, 4 and 8 ps for the overtone and the combination band, respectively, before setting into resonances. This behavior at non-fundamental resonances is related to the non-linear terms in the polarizability. It has been

discussed in our previous work [13, 14] and is also addressed in Section S.3 of the SI. The large amplitude oscillations of the symmetry-adapted stretching s_1 and bending s_2 coordinates confirm the assignment of the combination band as $\nu_2 + \nu_3$ (Figure 3), while the $2\nu_1$ overtone is properly characterized by a strongly increasing activity in the s_7 bending coordinate.

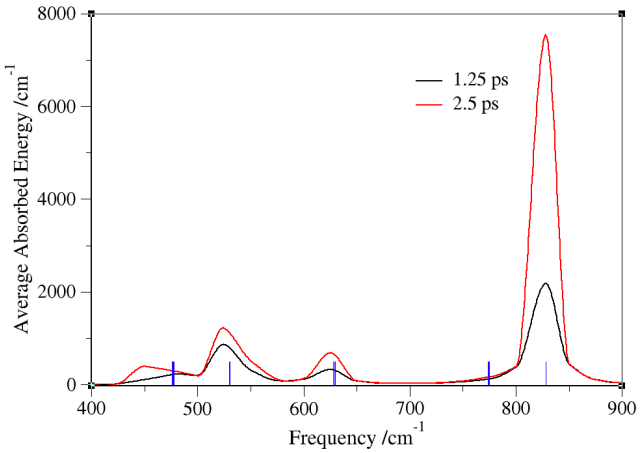

Figure 4. An illustration of the α-DMD facility as a Raman spectrum generating tool, here applied to C_{20} in the parallel regime at the B3LYP/6-31G(d) level of theory. The absorbed energies were recorded after 1.25 and 2.5 ps, respectively, and plotted as functions of the driven frequency with a resolution gauge of 25 cm^{-1}. The intensity of the electric field is 500 mV/bohr. The Raman-active frequencies in the double harmonic approximations are marked by blue sticks.

For the purposes of demonstrating the present first-principles based α-DMD approach to activating Raman modes in large polyatomics and clusters, we choose the smallest size carbon cluster that can form a closed fullerene molecule. Namely, C_{20} has been the subject of a number of theoretical studies at the level of density functional theory where it was shown that it can form multiple isomers of various shapes, including ring, bowl or cage [41-47]. The predicted relative stabilities of these isomers, however, appear to be quite sensitive to both the density functional and the basis set [45-47]. In the present work, we use the B3LYP functional, as it has produced the most consistent results for the fullerene, in conjunction with the 6-31G(d) orbital basis, with the polarization functions added for a proper description of the polarizability tensor. Tables S3 and S4

in the SI show the harmonic frequencies, IR, Raman intensities, and the XYZ coordinates of the optimized structure of C_{20}. We scanned the spectrum using the parallel Pump-Stokes alignment in the range from 400 cm^{-1} to 900 cm^{-1} with a 25 cm^{-1} gauge (a uniform frequency step). The spectrum is summarized in Figure 4, and the corresponding characteristic motion vectors and absorption profiles are shown in Figures S4-S5 in the SI. Clearly identifiable are the resonances at 450, 525, 625, and 828 cm^{-1} measured after 1.25 ps of exposure to the Pump field. The most Raman active, and by symmetry IR inactive, is the "breathing" mode at 828 cm^{-1}, also predicted as the most Raman active in the double-harmonic limit. Coordinate analysis, Figure 5, for this mode shows a well marked increase with time in the average sphere radius $\langle R(t)\rangle$ with a nearly constant radius fluctuation $\Delta R(t)$. Note also the steady increase in the polarizability, along with the energy profile (Figure S5), which indicates a 'clean' resonance with no detuning. The three other resonances are non-breathing type distortion modes, as is visible from the coordinate profiles in Figure 5, and all have much weaker Raman activity. Their polarizability and energy profiles indicate an initially clean absorption up to ~1 ps followed by a slowdown as the trajectory samples the non-harmonic parts of the potential and slightly detunes from the Pump frequency. All these resonances become more pronounced, while also acquiring anharmonic shifts, with a longer Pump field exposure time (2.5 ps). Such a systematic improvement in resolution was discussed previously by some of us in other applications [7]. This is especially noticeable for the peak near 450 cm^{-1}, a weakly Raman active mode, which becomes clearly identifiable only at the longer driving time and red-shifts from its harmonic frequency by ~30 cm^{-1}.

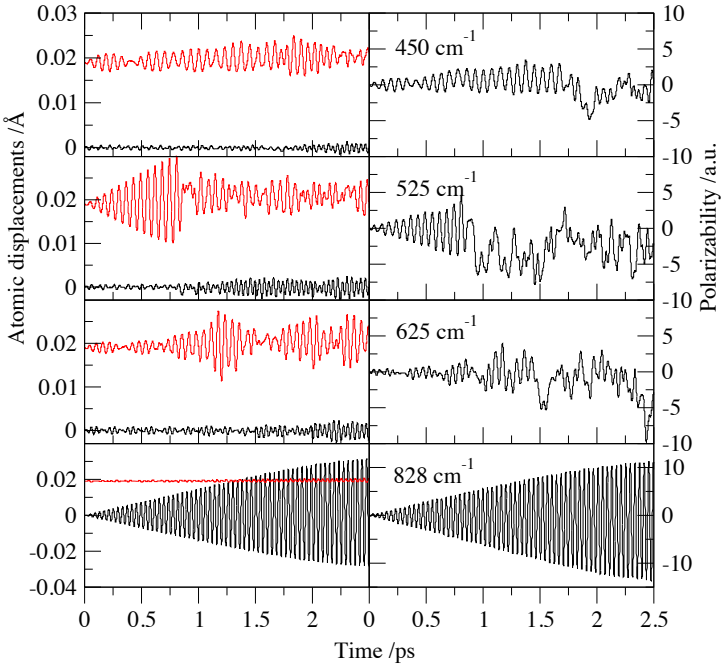

Figure 5. Average displacements, $\langle R(t)\rangle - \langle R(0)\rangle$ (in black), atomic fluctuations, $\Delta R(t) = \sqrt{\langle R(t)^2\rangle - \langle R(t)\rangle^2}$ (in red), and polarizability along the C_{20} α-DMD B3LYP/ 6-31G(d) trajectories for the most Raman active frequencies. The intensity of the electric field is 500 mV/bohr.

5. Concluding remarks

The DMD method described in the present paper is a first-time demonstration of the use of driven first-principles classical trajectories to stimulate Raman activity in molecules. We use two oscillating electric field vectors: a Pump with frequency ω_P and a Stokes probe with frequency ω_S, couple them to the molecule's polarizability and tune the Raman shift frequency $\omega = \omega_P - \omega_S$ to locate resonant vibrational excitations. A full Raman spectrum, including anharmonicities, combination bands, and overtones, can be constructed in this way, and what is particularly important, the resonances can be readily assigned to the corresponding molecular vibrations using the propagated trajectories. We also show that only one element of the full polarizability tensor, along with its nuclear derivative, is needed for an α-DMD trajectory, making this method suitable

for high-level *ab initio* molecular dynamics implementation, along with the already established direct *ab initio* dipole driven DMD approach. The theoretical foundation of the present method does not rely on any approximations beyond the electronic structure theory, i.e., the separation of nuclear and electronic motion, degree of electron correlation, basis set, etc. Numerical calculations performed at the MP2/cc-pVDZ and B3LYP/6-31G(d) levels of theory for H_2O, CH_4 and C_{20}, respectively, clearly demonstrate that the molecules absorb vibrational energy from the Pump field at fundamental frequencies, overtones, and combination bands. Application of α-DMD to other bulky and condensed and solid phase systems, such as transition metal clusters, carbon nanotubes and nanosheets, liquids, etc., for which the polarizability tensor is not readily available from the established models but may be calculated reasonably fast "on-the-fly", can provide valuable information about their vibrational structure in the Raman regime beyond the double harmonic approximation. For such systems, α-DMD should efficiently complement the existing direct plane wave DFT polarizability-polarizability correlation function approaches as a tool for spectra characterization.

It is also instructive to briefly explore the exciting possibility of studying energy flow dynamics by locating and "pumping", for example, a Raman active mode, such as the 828 cm^{-1} mode in C_{20}, and "probing" for IR activity in the prepared state. One may thus suggest novel computational techniques in designing 2-dimensional spectroscopy, for which experimental techniques already exist, [48] namely, pump-probe mixed IR-Raman, Raman-IR, Raman-Raman virtual experiments on determination of vibrational energy flow between IR and Raman active modes.

ACKNOWLEDGEMENTS

This work was supported by the National Science Foundation (Grants No. CHE–1855583 and DUE–1623723). This work was also supported in part by research computing resources and technical expertise via a partnership between Kennesaw State University's Office of the Vice President for Research and the Office of the CIO and Vice President for Information Technology [49].

REFERENCES

[1] R. B. Walker and R. K. Preston, J. Chem. Phys. **67**, 2017-2028 (1977).

[2] D-W. Noid and J.R. Stine, Chem. Phys. Lett. **65**, 153-157 (1979).

[3] D. W. Noid, C. Bottcher, and M. L. Koszykowski, Chem. Phys. Lett. **72**, 397-400 (1980).

[4] M. Christoffel and J. M. Bowman, J. Phys. Chem. **85**, 2159-2163 (1981).

[5] K. D. Hansel, Chem. Phys. Lett. **57**, 619-623 (1978).

[6] J. M. Bowman, X. Zhang, A. Brown, J. Chem. Phys. **119**, 646-650 (2003).

[7] M. Kaledin, A. Brown, A. L. Kaledin, J. M. Bowman, J. Chem. Phys. **121**, 5646-5653 (2004).

[8] A. L. Kaledin, M. Kaledin, J. M. Bowman, J. Chem. Theory Comput. **2**, 166-174 (2006).

[9] M. Kaledin, A. L. Kaledin, A. Brown, J. M. Bowman, In Normal-Mode Analysis: Theory and Applications to Biological and Chemical Systems; Q. Cui, I. Bahar, Eds.; CRC Press: Boca Raton, FL, (2005).

[10] M. Kaledin, A. L. Kaledin, J. M. Bowman, J. Dong, K. D. Jordan, J. Phys. Chem. A **113**, 7671-7677 (2009).

[11] M. Kaledin, J. M. Moffitt, C. R. Clark, F. Rizvi, J. Chem. Theory Comput. **5**, 1328-1336 (2009**).**

[12] T. Esser, H. Knorke, K.R. Asmis, W. Schollkopf, Q. Yu, C. Qu, J.M. Bowman, M. Kaledin, J. Phys. Chem. Lett. **9**, 798-803 (2018).

[13] R. Hooper, D. Boutwell, M. Kaledin, J. Phys Chem. A **123**, 5613-5620 (2019).

[14] D. Boutwell, O. Okere, O. Omodemi, A. Toledo, A. Barrios, M. Olocha, M. Kaledin J. Phys. Chem. A **124**, 7549-7558 (2020).

[15] M. Kaledin, A. L. Kaledin, J. M. Bowman, J. Phys. Chem. A **110**, 2933-2939 (2006).

[16] G. Niehues, A. L. Kaledin, J. M. Bowman, M. Havenith, J. Phys. Chem. B **116**, 10020-10025 (2012).

[17] B. J. Braams and J. M. Bowman, Int. Rev. Phys. Chem. **28**, 577-606 (2009).

[18] B. T. Thole, Chem. Phys. **59**, 341-350 (1981)..

[19] K. J. J. Miller, Am. Chem. Soc. **112**, 8533-8542 (1990).

[20] P. T. van Duijnen, M. J. Swart, J. Phys. Chem. A **102**, 2399-2407 (1998).

[21] P. Ren and J. W. Ponder, J. Phys. Chem. B **107**, 5933-5947 (2003).

[22] S. K. Reddy, D. R. Moberg, S. C. Straight and F. Paesani, J. Chem. Phys. **147**, 244504:1-9 (2017).

[23] G. R. Medders and F. Paesani, J. Chem. Theory Comput. **11**, 1145-1154 (2015).

[24] S. Luber, M. Iannuzzi, and J. Hutter, J. Chem. Phys. **141**, 094503:1-9 (2014).

[25] A. Putrino and M. Parrinello, Phys. Rev. Lett. **88**, 176401:1-4 (2002).

[26] M. Pagliai, C. Cavazzoni, G. Cardini, G. Erbacci, M. Parrinello, and V. Schettino, J. Chem. Phys. **128**, 224514:1-7 (2008).

[27] M. Brehm, M. Thomas, S. Gehrke, and B. Kirchner, J. Chem. Phys. **152**, 164105:1-21 (2020).

[28] D. A. McQuarrie, *Statistical Mechanics*; Harper & Row: New York, 1976.

[29] E. B. Wilson, J. C. Decius, P. C. Cross, *Molecular vibrations* (Dover, New York, 1980).

[30] One assumes here that the field energy is much smaller than the electronic excitation energy.

[31] A. Szabo and N. S. Ostlund, *Modern Quantum Chemistry: Introduction to Advanced Electronic Structure Theory* (Dover Publications, Inc., Mineola, NY, 1996).

[32] Y. X. Yan, E. B. Gamble, K. A. Nelson, J. Chem. Phys. **83**, 5391-5399 (1985).

[33] A. Laubereau and W. Kaiser, Rev. Mod. Phys. **50**, 607-665 (1978).

[34] G. P. Agrawal, In *Nonlinear Fiber Optics*, 6th ed. (Academic Press, Oxford, 2019).

[35] Y. M. Chang, L. Xu and H. W. K. Tom, Phys. Rev. Lett. **78**, 4649-4652 (1997).

[36] X. Huang, B. J. Braams, J. M. Bowman, J. Chem. Phys. **122**, 044308:1-12 (2005).

[37] H.-J. Werner, P. J. Knowles, G. Knizia, F. R. Manby and M. Schütz, WIREs Comput. Mol. Sci. **2**, 242-253 (2012).

[38] H.-J. Werner, P. J. Knowles, F. R. Manby, J. A. Black, K. Doll, A. Heßelmann, D. Kats, A. Köhn, T. Korona, D. A. Kreplin, Q. Ma, T. F. Miller, III, A. Mitrushchenkov, K. A. Peterson, I. Polyak, G. Rauhut, M. Sibaev J. Chem. Phys. **152**, 144107:1-24 (2020).

[39] MOLPRO, version 2019.2, a package of ab initio programs, H.-J. Werner, P. J. Knowles, G. Knizia, F. R. Manby, M. Schütz, P. Celani, W. Györffy, D. Kats, T. Korona, R. Lindh, A. Mitrushenkov, G. Rauhut, K. R. Shamasundar, T. B. Adler, R. D. Amos, S. J. Bennie, A. Bernhardsson, A. Berning, D. L. Cooper, M. J. O. Deegan, A. J. Dobbyn, F. Eckert, E. Goll, C. Hampel, A. Hesselmann, G. Hetzer, T. Hrenar, G. Jansen, C. Köppl, S. J. R. Lee, Y. Liu, A. W. Lloyd, Q. Ma, R. A. Mata, A. J. May, S. J. McNicholas, W. Meyer, T. F. Miller III, M. E. Mura, A. Nicklass, D. P. O'Neill, P. Palmieri, D. Peng, K. Pflüger, R. Pitzer, M. Reiher, T. Shiozaki, H. Stoll, A. J. Stone, R. Tarroni, T. Thorsteinsson, M. Wang, and M. Welborn, see https://www.molpro.net.

[40] Gaussian 16, Revision A.03, M. J. Frisch, G. W. Trucks, H. B. Schlegel, G. E. Scuseria, M. A. Robb, J. R. Cheeseman, G. Scalmani, V. Barone, G. A. Petersson, H. Nakatsuji, X. Li, M.

Caricato, A. V. Marenich, J. Bloino, B. G. Janesko, R. Gomperts, B. Mennucci, H. P. Hratchian, J. V. Ortiz, A. F. Izmaylov, J. L. Sonnenberg, D. Williams-Young, F. Ding, F. Lipparini, F. Egidi, J. Goings, B. Peng, A. Petrone, T. Henderson, D. Ranasinghe, V. G. Zakrzewski, J. Gao, N. Rega, G. Zheng, W. Liang, M. Hada, M. Ehara, K. Toyota, R. Fukuda, J. Hasegawa, M. Ishida, T. Nakajima, Y. Honda, O. Kitao, H. Nakai, T. Vreven, K. Throssell, J. A. Montgomery, Jr., J. E. Peralta, F. Ogliaro, M. J. Bearpark, J. J. Heyd, E. N. Brothers, K. N. Kudin, V. N. Staroverov, T. A. Keith, R. Kobayashi, J. Normand, K. Raghavachari, A. P. Rendell, J. C. Burant, S. S. Iyengar, J. Tomasi, M. Cossi, J. M. Millam, M. Klene, C. Adamo, R. Cammi, J. W. Ochterski, R. L. Martin, K. Morokuma, O. Farkas, J. B. Foresman, and D. J. Fox, Gaussian, Inc., Wallingford CT, 2016.

[41] V. Parasuk, J. Almlöf, Chem. Phys. Lett. **184**, 187-190 (1991).

[42] P. R. Taylor, E. Bylaska, J. H. Weare, R. Kawai, Chem. Phys. Lett. **235**, 558-563 (1995).

[43] Z. Wang, P. Day, R. Pachter, Chem. Phys. Lett. **248**, 121-126 (1996).

[44] S. Sokolova, A. Luchow, J. B. Anderson, Chem. Phys. Lett. **323,** 229-233 (2000).

[45] E. Malolepsza, H. A. Witek, S. Irle, J. Phys. Chem A **111**, 6649-6657 (2007).

[46] C. Zhang, W. Sun, Z. Cao, J. Chem. Phys. **126**, 144306: 1-7 (2007).

[47] D. M. Cleland, E. K. Fletcher, A. Kuperman, M. C. Per, J. Phys. Mater. **3**, 025006: 1-11 (2020).

[48] G. Mead, H.-W. Lin, I.-B. Magdău, T. F. Miller, III, and G. A. Blake, J. Phys. Chem. B **124**, 8904-8908 (2020).

[49] T. Boyle and A. Ramazan, Center for Research Computing, Kennesaw State University, 2021, Digital Commons Training Materials, 10.

https://digitalcommons.kennesaw.edu/training/10

Supporting Information

A Polarizability driven *ab initio* molecular dynamics approach to stimulating Raman activity: Application to C_{20}

Dominick Pierre-Jacques[1], Ciara Tyler[1], Jason Dyke[1], Alexey L. Kaledin[2] and Martina Kaledin[1,*]
[1] *Department of Chemistry & Biochemistry, Kennesaw State University, 370 Paulding Ave NW, Box # 1203, Kennesaw, GA 30144*
[2] *Cherry L. Emerson Center for Scientific Computation, Emory University, 1515 Dickey Drive, Atlanta, Georgia, 30322*

This document contains additional information, such as background theory, computational details and data that support mode assignment. **Tables S1-S4** show frequencies, IR and Raman intensities for H_2O, CH_4 and C_{20} molecules, respectively, and XYZ coordinates of C_{20}. **Figure S2** compares energy absorption regimes of Raman (α-DMD) versus IR (μ-DMD) for H_2O. Also, the definition of H_2O and CH_4 symmetry-adapted coordinates used for the trajectory analysis is given in **Eq. S4-1, S4-2** and shown in **Figure 1** of the main text and **Figure S3. Figure S4** shows C_{20} normal mode vectors of some Raman active modes. Average absorbed energies for most Raman active frequencies along the C_{20} α-DMD B3LYP/6-31G(d) trajectories are displayed in **Figure S5**.

Table of contents

Corresponding Author
*Email: mkaledin@kennesaw.edu (M.K.)

S1: The stimulated Raman energy term

Here we examine the stimulated Raman energy, Eq. 8, by expanding and reordering the corresponding cosine terms while setting $\phi_{\mathrm{P}} = \phi_{\mathrm{S}} = 0$ for compactness,

$$W_2(\mathbf{q},t) = \frac{\varepsilon_{\mathrm{P}}^2}{4}\alpha_{\mathrm{PP}}(\mathbf{q})\cos(2\omega_{\mathrm{P}}t) + \frac{\varepsilon_{\mathrm{S}}^2}{4}\alpha_{\mathrm{SS}}(\mathbf{q})\cos(2\omega_{\mathrm{S}}t) + \frac{\varepsilon_{\mathrm{P}}\varepsilon_{\mathrm{S}}}{2}\alpha_{\mathrm{PS}}(\mathbf{q})\cos\big((\omega_{\mathrm{P}}+\omega_{\mathrm{S}})t\big)$$
$$+ \frac{\varepsilon_{\mathrm{P}}\varepsilon_{\mathrm{S}}}{2}\alpha_{\mathrm{PS}}(\mathbf{q})\cos\big((\omega_{\mathrm{P}}-\omega_{\mathrm{S}})t\big) + \frac{\varepsilon_{\mathrm{P}}^2}{4}\alpha_{\mathrm{PP}}(\mathbf{q}) + \frac{\varepsilon_{\mathrm{S}}^2}{4}\alpha_{\mathrm{SS}}(\mathbf{q}) \qquad (\mathrm{S1}-1)$$

On the right-hand-side, the leading three terms are the vibrationally non-contributing waves resulting from sum-frequency mixing. While computationally possible to include them in the calculations by setting ω_{P} and ω_{S} to the laser frequencies used in a typical SRS experiment, their numerical contribution to the equations of motion, Eq. 9, will be negligible compared to the Stokes frequency term. Thus, these terms are neglected. The fourth term is the dominantly contributing Stokes-shifted vibrationally-resonant driving term. The last two terms appear as non-driving contributions to the induced-dipole-field energy and may actually be interpreted as the Rayleigh scattering components of the Pump and Stokes fields. In the parallel alignment regime, P=S, and the constant terms may be incorporated into the vibrationally resonant driving term. Their contribution to the internal energy of the molecule (Eq. 11), compared to any finite Stokes-shift vibrational frequency ω, occurs indirectly by perturbing the oscillator motion and will also be negligible. However, in the perpendicular alignment regime, they form a standalone term that theoretically should contribute to rotational energy absorption. Other cases when the Rayleigh terms can be important include driven systems with many very low frequency phonon-type vibrational modes, as those present in biological macromolecules, polymers or liquids. The exact contribution of the Raleigh terms will be examined in a future work.

S2: A 1-D harmonic oscillator with a linear polarizability term

For a harmonic oscillator of mass *m* in 1-D, the potential energy is

$$V(x) = \frac{1}{2} m\omega_0^2 x^2 \qquad (S2-1)$$

where ω_0 is the characteristic frequency. Expanding the polarizability in a Taylor series around the minimum energy point

$$\alpha(x) = \alpha_0 + \alpha_1 x + \frac{1}{2}\alpha_2 x^2 + \cdots \qquad (S2-2)$$

and keeping the two leading terms defines the so-called double harmonic approximation for Raman spectra, which is also the double-harmonic definition for the dipole moment function and the resulting dipole (infrared) spectra. Substitution of Eq. S2-2 into Eq. 9 leads to a second-order linear differential equation for the coordinate,

$$\ddot{x} + \omega_0^2 x = \gamma \cos(\omega t + \theta) \qquad (S2-3)$$

where $\gamma = -\varepsilon_0^2 \alpha_1 / 2m$. If the driving frequency ω coincides with the characteristic frequency ω_0, this equation has the following solution,

$$x(t) = \left(\frac{\gamma t}{2\omega_0} + A\right)\sin(\omega_0 t + \theta) + \left(\frac{\gamma}{4\omega_0^2} + B\right)\cos(\omega_0 t + \theta) \qquad (S2-4.1)$$

and the momentum,

$$p(t) = m\left(\frac{\gamma}{4\omega_0} - \omega_0 B\right)\sin(\omega_0 t + \theta) + m\left(\frac{\gamma t}{4} + \omega_0 A\right)\cos(\omega_0 t + \theta) \qquad (S2-4.2)$$

with *A* and *B* defined by the initial conditions. For a specific case with the system initially at rest, as considered in the numerical calculations in the present work, and setting $\theta = 0$, as required by Eq. 8, the coordinate and momenta become, respectively,

$$x(t) = \frac{\gamma t}{2\omega_0}\sin\omega_0 t \qquad (S2-5.1)$$

and

$$p(t) = \frac{m\gamma t}{2}\cos\omega_0 t + \frac{m\gamma}{2\omega_0}\sin\omega_0 t \qquad (S2-5.2)$$

Using Eqs. S2-5 and Eq. 11, the average absorbed internal energy as a function of time is

$$\langle H_0(t)\rangle = \frac{1}{t}\int_0^t dt'\left(\frac{p^2(t')}{2m} + \frac{m\omega_0^2 x^2(t')}{2}\right) \qquad (S2-6)$$

and after the integration and some manipulation, it simplifies to

$$\langle H_0(t)\rangle = E_0^{(\alpha)}\omega_0^2 t^2[1 + 3\mathrm{sinc}^2(\omega_0 t)] \qquad (S2-7)$$

with the characteristic polarizability energy

$$E_0^{(\alpha)} = \frac{\varepsilon_0^4\alpha_1^2}{96m\omega_0^2} \qquad (S2-8.1)$$

Similarly, for dipole driving, with $\gamma = -\varepsilon_0\mu_1/m$, the characteristic dipole energy is

$$E_0^{(\mu)} = \frac{\varepsilon_0^2\mu_1^2}{24m\omega_0^2} \qquad (S2-8.2)$$

where μ_1 is the dipole derivative.

In a resonant steady state, with $t \gg \sqrt{3}/\omega_0$, the oscillating term in the square brackets of Eq. S2-7 is much smaller than the unity, and hence the internal energy increases quadratically with time as

$$\langle H_0(t)\rangle \approx E_0^{(\alpha)}\omega_0^2 t^2 \qquad (S2-9)$$

Equations S2-7 - S2-9 have two implications for resonantly driving a generic polyatomic molecule in either Raman or infrared (dipole driven) regimes: (i) steady state conditions are reached slower at lower frequencies, i.e. one needs longer driving times at lower frequency fundamentals than at higher ones to identify a resonance, and (ii) the response of the molecule to the incident Raman field is much more sensitive to the field strength than that of the dipole field, that is, in DMD

simulations one will always need much stronger electric fields to induce Raman active resonances than dipole active resonances, both in the form of energy absorption.

S.3: 1-D and 2-D harmonic oscillators with a quadratic polarizability term

It is instructive to examine the role of the higher order terms in Eq. S2-2. Assuming the quadratic term while neglecting the linear term results in the following equation for the coordinate

$$\ddot{x} + \left(1 - \frac{\gamma}{\omega_0^2}\cos(\omega t)\right)\omega_0^2 x = 0 \qquad (S3-1)$$

where $\gamma = -\varepsilon_0^2\alpha_2/2m$. This is a case of a parametric oscillator, i.e., one with a variable characteristic frequency, $\omega_0(t)$, and one that has the solutions in terms of Mathieu's functions [1]

$$x(t) = A_1 \mathrm{Ce}\left(\frac{\omega_0}{\omega}, \gamma, t\right) + A_2 \mathrm{Se}\left(\frac{\omega_0}{\omega}, \gamma, t\right) \qquad (S3-2)$$

with the coefficients A_1, A_2 determined by the initial conditions. Eq. S3-2 is convergent for all values of t except in the special, resonant case where the field frequency is $\omega = 2\omega_0$, corresponding to the overtone excitation. At such a resonance, the coordinate and the internal energy increase exponentially with t, unlike linearly and quadratically, respectively, at a fundamental resonance. In other words, classically driving the molecule at an overtone frequency will result in a resonant absorption as long as α_2, and similarly μ_2 in dipole driving, are non-zero. This is demonstrated graphically in Figure S1 where we show a parallel Pump-Stokes polarization calculation of H_2 at the overtone frequency $2\omega_0$. As can be seen, following an initial delay of ~0.5 ps, the energy begins to increase rapidly at an exponential rate. The 'pre-resonance' delay time is determined by polarizability's second derivative, α_2, an intrinsic molecular property, and much more sensitively by the field strength ε_0, an external tunable parameter.

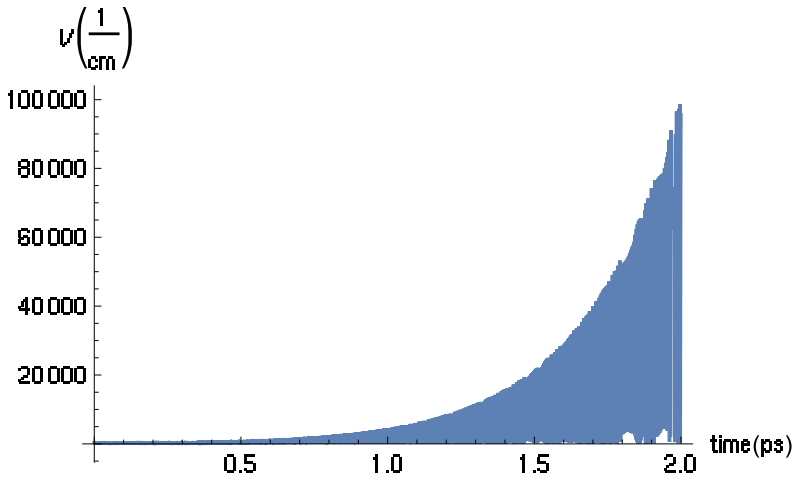

Figure S1. The potential energy V of a 1-D harmonic oscillator driven by a Pump electric field of the frequency corresponding to the first overtone and coupled to quadratic polarizability (see Eq. 8): $W_2(x,t) = \varepsilon_0^2 \alpha_2 x^2 \cos(2\omega_0 t)/4$. In this example, the represented system is H_2, calculated at the MP2/cc-pVDZ level of with the following parameters: ω_0=4502 cm^{-1}, α_2=-4.166 a.u., ε_0=1 V/bohr. (The solution and graphics are generated with the Mathematica software. [2])

We now consider a simple case of coupled excitations using a two-dimensional harmonic oscillator,

$$V(x,y) = \frac{1}{2} m(\omega_1^2 x^2 + \omega_2^2 y^2) \qquad (S3-3)$$

with the characteristic frequencies ω_1 and ω_2, and the corresponding polarizability function,

$$\alpha(x,y) = \alpha_0 + \alpha_x x + \alpha_y y + \frac{1}{2}\alpha_{xx} x^2 + \frac{1}{2}\alpha_{yy} y^2 + \alpha_{xy} xy + \cdots \qquad (S3-4)$$

We have shown above that α_x, α_y (α_1 in 1-D) are responsible for the fundamental resonances ($\omega=\omega_0$), while α_{xx} and α_{yy} (α_2 in 1-D) are responsible for the double excitations, i.e. overtones ($\omega=2\omega_0$). If we retain only the α_{xy} term from Eq. S3-4 and write out the equations of motion, we obtain a set of coupled ODEs,

$$\ddot{x} + \omega_1^2 x - \gamma \cos(\omega t)\, y = 0 \qquad (S3-5.1)$$

$$\ddot{y} + \omega_2^2 y - \gamma \cos(\omega t)\, x = 0 \qquad (S3-5.2)$$

with $\gamma = -\varepsilon_0^2 \alpha_{xy}/2m$. A unitary transformation may decoupled these equations to variables (u,v) by solving the secular equation, for each of its eigenvalues $\lambda_j, j = 1,2$,

$$\begin{pmatrix} 0 & -\gamma\cos(\omega t) \\ -\gamma\cos(\omega t) & \omega_2^2 - \omega_1^2 \end{pmatrix} \begin{pmatrix} c_{j1} \\ c_{j2} \end{pmatrix} = \lambda_j \begin{pmatrix} c_{j1} \\ c_{j2} \end{pmatrix} \qquad (S3-6)$$

Now, by the construction of the driving force term, $\alpha(x,y) \equiv \alpha_{xy} xy$, neither the fundamentals nor the overtones can be excited in Eqs. S3-5; thus, it is sufficient to demonstrate the occurrence of a combination resonance by setting $\omega_1=\omega_2=\omega_0$ (while also greatly simplifying the solution of S3-5, S3-6). With this choice, the transformation matrix is time-independent, i.e., $u = (x-y)/\sqrt{2}$ and $v = (x+y)/\sqrt{2}$. The de-coupled system of ODEs is

$$\ddot{u} + \omega_0^2 u + \gamma\cos(\omega t)\, u = 0 \qquad (S3-7.1)$$

$$\ddot{v} + \omega_0^2 v - \gamma\cos(\omega t)\, v = 0 \qquad (S3-7.2)$$

with the solutions appearing in the form of Eq. S3-2; back-transformation to (x,y) is trivial from here. Therefore, as argued above, both oscillators exhibit resonant behavior at the external field frequency $\omega = 2\omega_0$, corresponding here to the $\omega_1+\omega_2$ combination band rather than to one of the overtones. We note that this resonance occurs even in the absence of an explicit coupling term between x and y, as given by Eq S3-3. Thus, driving a polyatomic molecule at a frequency of a combination band of any two fundamentals is also a form o parametric oscillator resonance. This proves that the polarizability term α_{xy}, and the corresponding dipole term μ_{xy}, are responsible for exciting combination bands in classical DMD.

S.4. Details of Calculations

Table S1. H_2O Harmonic vibrational frequencies (in cm^{-1}), IR intensities (km/mol), and Raman intensities ($Å^4$/amu) calculated at the MP2/cc-pVDZ level of theory.

Label	Frequency	IR intensity	Raman intensity
$\nu_1(A_1)$	1677	57.0	5.8
$\nu_2(A_1)$	3852	6.6	68.3
$\nu_3(B_2)$	3971	32.6	33.8

The symmetry-adapted coordinates for H_2O are

$$s_1(A_1) = 2^{-\frac{1}{2}}(\Delta r_1 + \Delta r_2)$$

$$s_2(B_2) = 2^{-\frac{1}{2}}(\Delta r_1 - \Delta r_2))$$

$$s_3(A_1) = \Delta\alpha_{12} \qquad \text{(S4-1)}$$

where Δr_i indicate the O-H_i bond length fluctuations and $\Delta\alpha_{ij}$ indicate the H_i-O-H_j angle fluctuations.

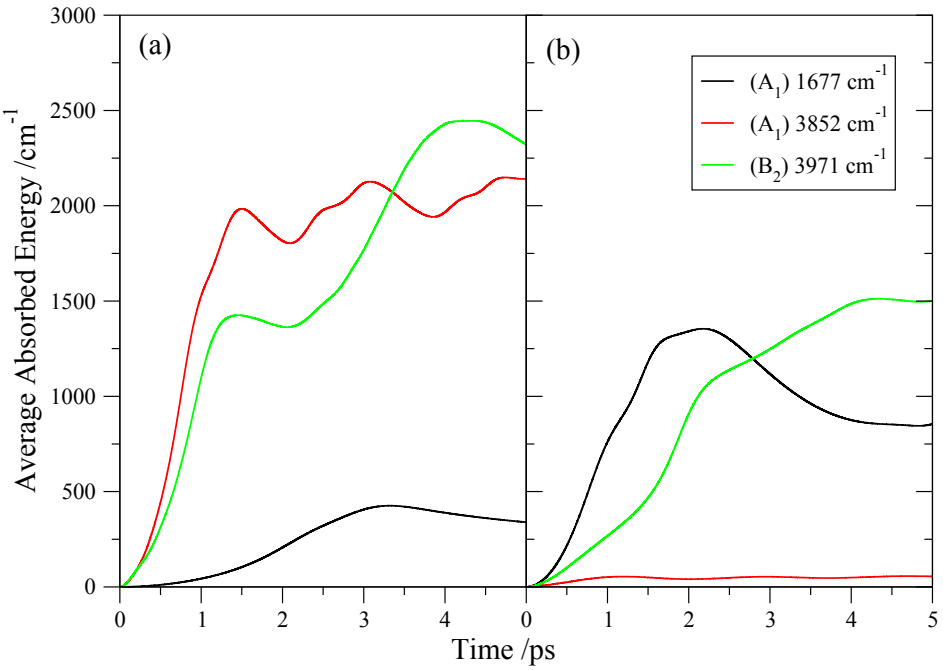

Figure S2. An α-DMD (a) and μ-DMD (b) energy absorption comparison of the H_2O fundamental modes $\nu_1(A_1)$=1677cm^{-1}, $\nu_2(A_1)$=3852 cm^{-1}, and $\nu_3(B_2)$=3971 cm^{-1}. The intensity of the electric field was 500 and 100 mV/bohr, respectively. The level of theory is MP2/cc-PVDZ.

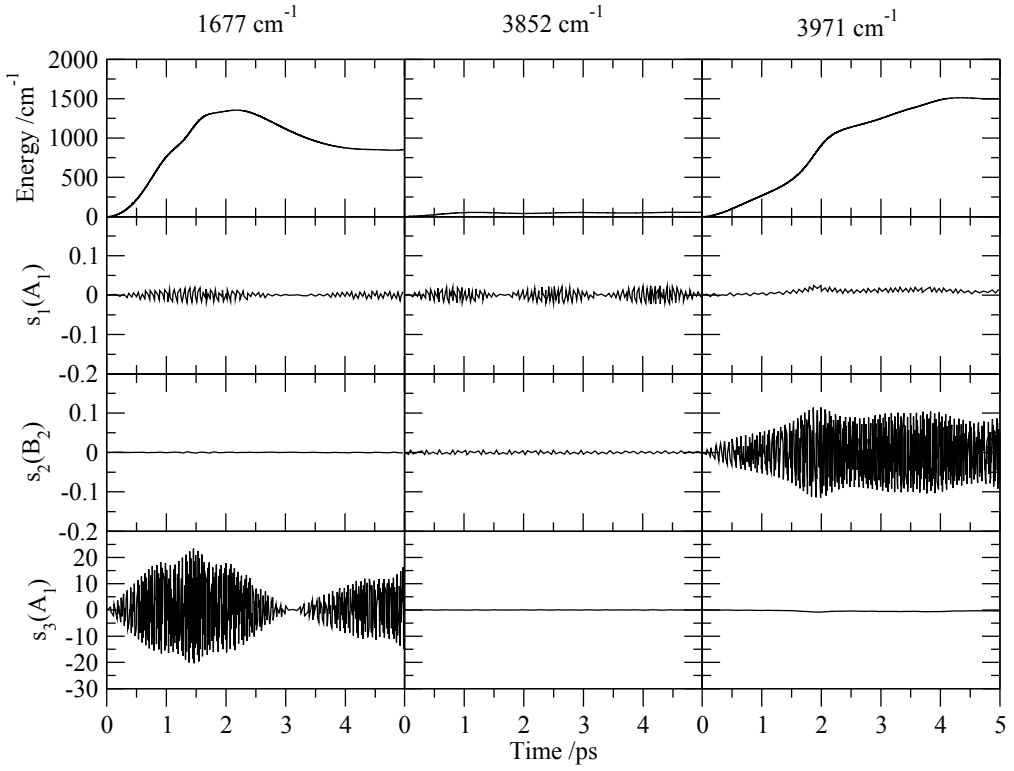

Figure S3. Direct μ-DMD trajectory analysis for the IR active H_2O fundamental frequencies $\nu_1(A_1)$=1677 cm^{-1}, $\nu_2(A_1)$=3852 cm^{-1}, and $\nu_3(B_2)$=3971 cm^{-1}. Average absorbed energies are in cm^{-1}, symmetry-adapted coordinates s_1 and s_2 in Å, and s_3 in degrees. The intensity of the electric field was 100 mV/bohr.

Table S2. The CH_4 Harmonic vibrational frequencies (in cm^{-1}), IR intensities (km/mol), and Raman intensities ($Å^4$/amu) calculated at the MP2/cc-pVDZ level of theory.

Label	Frequency	IR intensity	Raman intensity
ν_1 (T_2)	1338	11.5	1.2
ν_2 (E)	1565	0.0	21.0
ν_3 (A_1)	3082	0.0	144.4
ν_4 (T_2)	3233	17.0	59.9

The symmetry-adapted coordinates for CH_4 are [3]

$$s_1(A_1) = 4^{-\frac{1}{2}}(\Delta r_1 + \Delta r_2 + \Delta r_3 + \Delta r_4)$$
$$s_2(E) = 12^{-\frac{1}{2}}(2\Delta\alpha_{23} + 2\Delta\alpha_{45} - \Delta\alpha_{25} - \Delta\alpha_{34} - \Delta\alpha_{35} - \Delta\alpha_{24})$$
$$s_3(E) = 4^{-\frac{1}{2}}(\Delta\alpha_{25} + \Delta\alpha_{34} - \Delta\alpha_{35} - \Delta\alpha_{24})$$
$$s_4(T_2) = 4^{-\frac{1}{2}}(\Delta r_1 - \Delta r_2 + \Delta r_3 - \Delta r_4)$$
$$s_5(T_2) = 4^{-\frac{1}{2}}(-\Delta r_1 + \Delta r_2 + \Delta r_3 - \Delta r_4)$$
$$s_6(T_2) = 4^{-\frac{1}{2}}(\Delta r_1 + \Delta r_2 - \Delta r_3 - \Delta r_4)$$
$$s_7(T_2) = 2^{-\frac{1}{2}}(\Delta\alpha_{25} - \Delta\alpha_{34})$$
$$s_8(T_2) = 2^{-\frac{1}{2}}(\Delta\alpha_{35} - \Delta\alpha_{24})$$
$$s_9(T_2) = 2^{-\frac{1}{2}}(\Delta\alpha_{23} - \Delta\alpha_{54}) \quad \text{(S4-2)}$$

where 1,2,3,4 subscripts denote hydrogens, Δr_i indicates the C-H_i bond length fluctuation and $\Delta\alpha_{ij}$ indicates the H_i-C-H_j angle fluctuation.

Table S3. C_{20} (C_i symmetry) harmonic vibrational frequencies (in cm^{-1}), IR intensities (km/mol), and Raman intensities ($Å^4$/amu) calculated at the B3LYP/6-31G(d) level of theory.

Freq	IR int.	Freq	Raman int.
508	20.2	68	20.2
545	0.0	81	20.0
571	0.1	309	0.0
571	0.2	477	41.8
604	0.2	478	41.3
606	3.2	530	22.1
608	3.0	629	14.1
633	2.8	631	13.7
634	3.0	723	0.0
640	1.4	761	0.2
723	36.6	775	0.9
723	37.2	775	0.9
892	19.5	829	83.9
923	5.6	1009	4.3
924	5.4	1010	4.3
1091	6.9	1129	4.2
1166	1.2	1130	4.5
1166	1.1	1177	2.0
1174	0.0	1232	4.9
1208	6.2	1237	0.0
1208	6.9	1295	4.2
1256	2.0	1297	3.3
1289	4.1	1315	4.7
1290	3.3	1317	5.5
1352	0.1	1420	15.8
1362	96.5	1443	15.0
1364	97.0	1444	15.1

Table S4. XYZ coordinates (Å) for the C_{20} C_i minimum, calculated with B3LYP/6-31G(d).

Atom	X	Y	Z
C	1.9571458647	-0.0033079274	-0.7023708720
C	1.9570258915	0.0041158301	0.7027334273
C	-1.9570258915	-0.0041158301	-0.7027334273
C	-1.9571458647	0.0033079274	0.7023708720
C	0.0003224516	-0.7513029918	-1.8312161769
C	-0.0000217048	-0.6926756872	1.8153973200
C	0.0000217048	0.6926756872	-1.8153973200
C	-0.0003224516	0.7513029918	1.8312161769
C	-0.7583182954	-1.9361178192	-0.0360970821
C	-0.7591245359	1.9358041090	0.0359573441
C	0.7591245359	-1.9358041090	-0.0359573441
C	0.7583182954	1.9361178192	0.0360970821
C	1.1979971467	-1.2300241810	-1.1693292005
C	1.1732602928	1.1479543054	-1.1072440672
C	1.1735349864	-1.1474682310	1.1074593705
C	1.1972744660	1.2305179128	1.1695490126
C	-1.1972744660	-1.2305179128	-1.1695490126
C	-1.1735349864	1.1474682310	-1.1074593705
C	-1.1732602928	-1.1479543054	1.1072440672
C	-1.1979971467	1.2300241810	1.1693292005

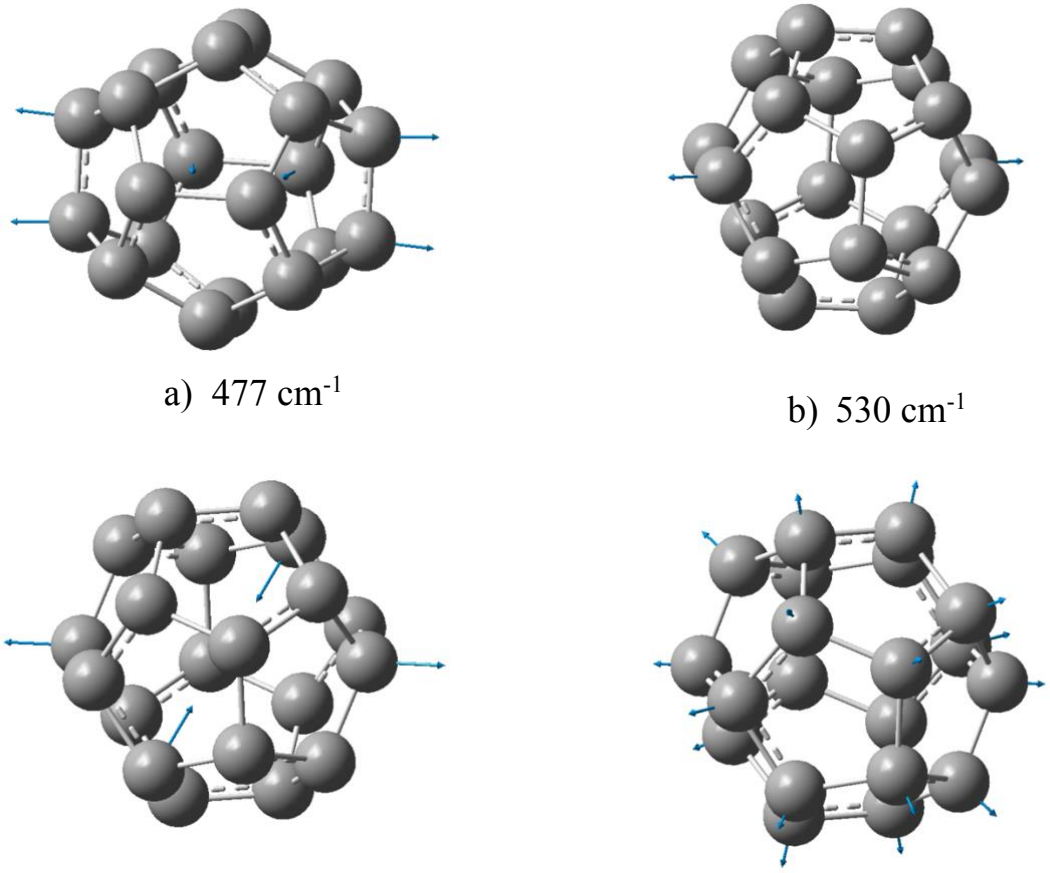

Figure S4. C_{20} normal modes vectors for some Raman active modes in the range from 400 to 900 cm^{-1}.

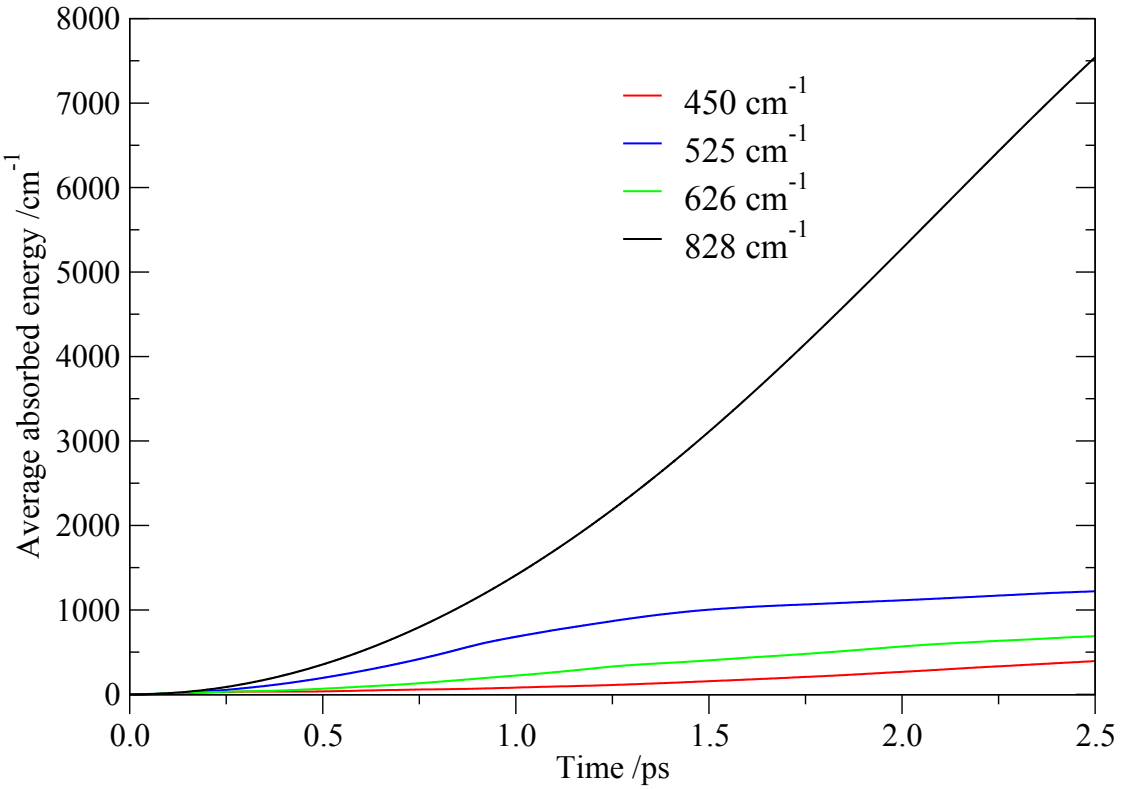

Figure S5. Average absorbed energies (in cm^{-1}) along the C_{20} α-DMD B3LYP/ 6-31G(d) trajectories for most Raman active frequencies. The intensity of the electric field was 500 mV/bohr.

References

[1] F. Arscott "Periodic differential equations: an introduction to Mathieu, Lamé, and allied functions" Pergamon Press: 1964.

[2] Wolfram Research, Inc., Mathematica, Version 12.0.0, Champaign, IL (2019).

[3] J. T. Hougen, G. Wiersma, Methane Symmetry Operations. NIST Physical Measurement Laboratory, Special Publications & Tutorials, **2016** (Access date: May 11, 2021). https://www.nist.gov/pml/methane-symmetry-operations